Sculpturing coherent states to get highly excited Fock states for stationary and travelling fields

INSTITUTE OF PHYSICS PUBLISHING JOURNAL OF OPTICS B: QUANTUM AND SEMICLASSICAL OPTICS

J. Opt. B: Quantum Semiclass. Opt. **6** (2004) 351–359 PII: S1464-4266(04)78068-4

Sculpturing coherent states to get highly excited Fock states for stationary and travelling fields

L P A Maia[1], B Baseia[1], A T Avelar[2] and J M C Malbouisson[3,4]

[1] Instituto de Física, Universidade Federal de Goiás, 74.001-970, Goiânia, GO, Brazil
[2] Instituto de Física, Universidade de Brasília, 70.001-970, Brasília, DF, Brazil
[3] Department of Physics, University of Alberta, Edmonton, AB, T6G 2J1, Canada

E-mail: jmalbou@phys.ualberta.ca

Received 19 March 2004, accepted for publication 12 May 2004
Published 8 June 2004
Online at stacks.iop.org/JOptB/6/351
doi:10.1088/1464-4266/6/7/013

Abstract
An adapted sequential application of dispersive atom–field interaction is used to engineer a field in a highly excited Fock state. A few atoms are used to group into a number component all photons inside a microwave cavity which initially contains a coherent state. The scheme differs from those adding photons to an empty cavity via successive passage of resonant atoms. A conveniently equipped sequence of Mach–Zehnder interferometers is found to be the complementary scheme, extending the result for (optical) travelling waves.

Keywords: quantum state engineering, number states

1. Introduction

Quantum state engineering has become an important issue in the last decade, both for field and atomic states, in view of recent theoretical and technological progress. For quantum optics, among the various advances one may cite teleportation [1], quantum computation [2], quantum communication [3] and quantum cryptography [4] as remarkable examples illustrating developments requiring the construction of convenient field states. Specific examples are found in [5, 6] where the construction of the *reciprocal binomial state* [7] plays a crucial role for experimentally determining the phase distribution of arbitrary states [5] and for quantum lithography [6]. A similar role is played by the *polynomial state* [8] and by the *complementary coherent state* [9] for measurement of quadrature variances and the Husimi Q-function, respectively [10]. Now, the state to be tailored may concern with either stationary or travelling waves. In the first case, engineering can be implemented via resonant [11] or dispersive [12] atom–field interaction, but sometimes a combination of these two schemes is required to get a desired state [7]. In the second case, the usual procedure employs a convenient array of beam-splitters [13], but alternative schemes can also be considered, e.g., using optical-fibres [14], four-wave mixing [15], intra-cavity second-harmonic generation [16], etc.

This work treats the generation of number states in two distinct scenarios. The first one is concerned with a field trapped inside a high-Q cavity, having a coherent state previously prepared in it, while the second scenario refers to a free running wave. In the case of trapped waves the field belongs to the microwave range whereas in the second situation, dealing with running waves, it may include the optical domain. In both cases we will employ quantum non-demolition procedures, using either dispersive atom–field interactions [12] or effective field–field interactions implemented by a non-linear medium [17]. Previous proposals preparing Fock states for stationary [18] and travelling waves [19] can be found in the literature. Experimental results for the states $|1\rangle$ and $|2\rangle$ in a microwave cavity are given in [20] and [21], respectively. A new experimental scheme, also for stationary microwaves, was proposed for the generation of a 'large' number state ($n = 6$) in [22]. Any reliable process must involve few fast steps due to decoherence effects.

[4] Permanent address: Instituto de Física, Universidade Federal da Bahia, 40210-340, Salvador, BA, Brazil.

Also, maintaining the large $|n\rangle$ state created faces a crucial difficulty due to decoherence [23], since the constructed state loses its integrity roughly during the decoherence time $t_d \propto 1/n$. However, one hopes that sideways procedures combined with rapid advance of the technology could circumvent such a problem in the near future.

With regard to the stationary case, a coherent state $|\alpha\rangle$, initially prepared inside the cavity, will be sculptured by the successive atoms, crossing the cavity one by one, ending up by grouping all the photons in the cavity onto a single component $|n\rangle$ of the Fock basis. This result can be verified by either monitoring the Wigner function of the resulting state or by looking at its photon-number distribution $P(n) = |\langle n|\Psi\rangle|^2$, which corresponds to the fidelity between the state $|\Psi\rangle$ and the Fock state $|n\rangle$. Here the latter choice provides an easier identification of the number state being sculptured, which occurs when $P(n)$ tends to a Kronecker delta. During the process of the passage of the atoms the initial coherent state is transformed, step by step, into *superpositions of circular coherent states* (SCCSs) which, by appropriate choice of parameters, become some specific number states.

With regard to the second case, the creation of a Fock state for travelling fields employs a different scheme, realized as a sequence of Mach–Zehnder interferometers including a (nonlinear) Kerr medium in one of their arms. A connection between the schemes for stationary and running fields is established, showing that the latter is the complement of the former, in the sense that there exist a map (step by step) between them, allowing us to extend the result obtained for stationary states to the case of travelling fields.

Earlier works [24, 25] have shown that circular coherent states form a good basis to represent quantum states, in particular Fock states. These ideas have inspired the investigation of even circular states [26] and the production of number states referring to the centre of mass vibrational motion of ions [27]. Here, we employ dispersive interactions and conditional measurements to generate a specific SCCS which reproduces highly excited number states of the kind $|2^N\rangle$ with a high fidelity.

This paper is arranged as follows. In section 2 we discuss the generation of SCCSs, both for stationary fields trapped inside cavities and for free fields in travelling waves, and comment on the analogy between these two situations. In section 3, by analysing the photon-number distributions of SCCSs, we discuss the generation of some highly excited Fock states (searching for an adequate choice of the parameters involved) and illustrate the evolution of the sculpturing process of an initial coherent state. The last section contains our conclusions.

2. Generation of SCCS

As we shall see, some highly excited Fock states can be produced as specific SCCSs with appropriate parameters. Before, we show how the SCCSs can be generated both as stationary states and as travelling waves.

2.1. Generation of SCCS in a cavity

A stationary field in an SCCS can be produced inside a microwave cavity, starting from a single-mode coherent state

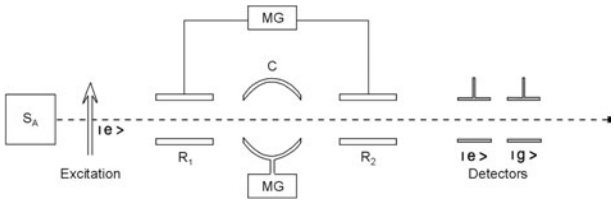

Figure 1. Schematic illustration of the experimental set-up for production of an SCCS in a high-quality cavity using dispersive atomic probes.

Table 1. Evolution of the atom–field state as the first atom crosses the system.

	$\|\Psi\rangle_{\text{atom+field}}$
Before R_1:	$\|e\rangle_1\|\alpha\rangle$
After R_1:	$(\|g\rangle_1 + \|e\rangle_1)\|\alpha\rangle$
After C:	$\|g\rangle_1\|\alpha\rangle + \|e\rangle_1\|e^{i\theta_1}\alpha\rangle$
After R_2:	$\|g\rangle_1(\|e^{i\theta_1}\alpha\rangle + \|\alpha\rangle) + \|e\rangle_1(\|e^{i\theta_1}\alpha\rangle - \|\alpha\rangle)$

initially prepared in it. The scheme is based on a (non-unitary) projection onto a field state, via selective atomic detection, of an entangled state-vector describing the atom–field system. The procedure constitutes an extension of others in the literature [12]. The reliability of the method requires the use of a high-Q superconducting cavity C, placed between two low-Q cavities (Ramsey zones R_1 and R_2), as schematically shown in figure 1.

Rydberg atoms, being ejected one by one with selected velocities from a source S_A, are prepared in a circular excited state $|e\rangle$ (principal quantum number $n = 51$ in the case of rubidium) by an appropriate laser beam. When atoms cross both Ramsey zones R_1 and R_2 they interact with classical fields produced by a microwave generator (MG). These interactions are resonant with the atomic transition between the states $|e\rangle$ and $|g\rangle$ ($n = 50$), the field intensities being adjusted to produce a $\pi/2$ rotation in the atomic space, that is,

$$|e\rangle \longrightarrow (|g\rangle + |e\rangle)/\sqrt{2}, \tag{1}$$

$$|g\rangle \longrightarrow (|g\rangle - |e\rangle)/\sqrt{2}. \tag{2}$$

A third (auxiliary) atomic level $|i\rangle$ ($n = 52$) is crucial in the scheme: the cavity frequency is adjusted close to resonance (detuned by small δ) with the transition $|e\rangle \longrightarrow |i\rangle$, but far from the transition $|g\rangle \longrightarrow |e\rangle$. The number of photons in the field being forbidden to change, only the phase may vary; so, concerning the transition $|g\rangle \longleftrightarrow |e\rangle$, the atom–field interaction in C is dispersive, instead of resonant. Such an interaction is described by the effective atom–field Hamiltonian [28],

$$H_{\text{int}} = \hbar\omega_{\text{eff}}\hat{a}^\dagger\hat{a}(|i\rangle\langle i| - |e\rangle\langle e|), \tag{3}$$

with $\omega_{\text{eff}} = 2d^2/\delta$ and d the atomic dipole moment. Thus the atom crossing the cavity produces a phase-shift in the field state when it is in the excited state $|e\rangle$, but no phase-shift appears when the atom is in the ground state $|g\rangle$.

Consider that the field in the high-Q cavity is initially in a coherent state $|\alpha\rangle$. The evolution of the entangled atom–field state, as the first atom crosses the system, follows the steps (apart from normalization and using $e^{i\phi\hat{a}^\dagger\hat{a}}|\alpha\rangle = |e^{i\phi}\alpha\rangle$)

Table 2. Evolution of the atom–field state during the passage of the second atom through the system.

	$\|\Psi\rangle_{\text{atom+field}}$
Before R_1:	$\|e\rangle_2(\|e^{i\theta_1}\alpha\rangle + \|\alpha\rangle)$
After R_1:	$(\|g\rangle_2 + \|e\rangle_2)(\|e^{i\theta_1}\alpha\rangle + \|\alpha\rangle)$
After C:	$\|g\rangle_2(\|e^{i\theta_1}\alpha\rangle + \|\alpha\rangle) + \|e\rangle_2(\|e^{i(\theta_1+\theta_2)}\alpha\rangle + \|e^{i\theta_1}\alpha\rangle)$
After R_2:	$\|g\rangle_2[\|e^{i\theta_1}\alpha\rangle + \|\alpha\rangle + \|e^{i(\theta_1+\theta_2)}\alpha\rangle + \|e^{i\theta_2}\alpha\rangle] + \|e\rangle_2[-\|e^{i\theta_1}\alpha\rangle - \|\alpha\rangle + \|e^{i(\theta_1+\theta_2)}\alpha\rangle + \|e^{i\theta_1}\alpha\rangle]$.

presented in table 1, where the subscript 1 refers to the first atom and $\theta_1 = \omega_{\text{eff}} t_1$, t_1 being the time the atom takes to cross the cavity. One sees that, if this first atom is detected in the state $|g\rangle$ ($|e\rangle$), the field in the cavity is projected onto the state $|e^{i\theta_1}\alpha\rangle + |\alpha\rangle$ ($|e^{i\theta_1}\alpha\rangle - |\alpha\rangle$). For our purpose, we take the detection to be that of the ground state $|g\rangle$.

Now assume that a second atom is ejected soon after the detection of the first one in $|g\rangle$; thus, for the passage of the second atom, the initial field state in the cavity is $|e^{i\theta_1}\alpha\rangle + |\alpha\rangle$, corresponding to the state projected by the detection of the first atom. In this circumstance, the atom–field state evolves as shown in table 2.

We see that the detection of the second atom, again in $|g\rangle$, leads to a superposition of the state $|e^{i\theta_1}\alpha\rangle + |\alpha\rangle$ with the rotated (by θ_2) partner $|e^{i\theta_1}\alpha\rangle - |\alpha\rangle$. Proceeding in this way, after the passage of N atoms through the system, controlling their velocities such that $\theta_1 = \theta, \theta_2 = \theta/2, \ldots, \theta_N = \theta/2^{N-1}$ and all of them being detected in the state $|g\rangle$, the state generated in the cavity is

$$|\Psi_N(\alpha,\theta)\rangle = \mathcal{N}_N(\alpha,\theta)\sum_{j=0}^{J_N}\left(|e^{i\theta}\alpha_j\rangle + |\alpha_j\rangle\right), \qquad (4)$$

where $\alpha_j = \alpha\exp(i\theta j/2^{N-1})$ and $J_N = 2^{N-1} - 1$, $\mathcal{N}_N(\alpha,\theta)$ standing for the normalization factor. The coherent states participating in the superposition state (4) can be represented by equally separated points over the circle of radius $|\alpha|$ in the complex plane, ranging in the interval $[\theta_0, \theta_0 + 2\theta(1 - 2^{-N})]$ where $\theta_0 = \arg(\alpha)$. If one takes N infinitely large then these points are an enumerable (rational) cover of the interval (arc) $[\theta_0, \theta_0 + 2\theta)$; without loss of generality, we take α to be real and positive ($\theta_0 = 0$) from now on. Notice that, fixing $\theta = \pi$, one recovers the symmetrical case studied in [29], which is an even state in the sense that $|\Psi_N(-\alpha,\pi)\rangle = |\Psi_N(\alpha,\pi)\rangle$.

2.2. Generation of SCCS as travelling modes

The superposition states (4) can also be produced as running waves of the electromagnetic field. The generation scheme is complementary to the preceding one in the sense that they can be mapped, step by step, into one another. It consists of a set of Mach–Zehnder interferometers (MZIs), all of them fed with a Fock state $|1\rangle$ and the vacuum in the internal modes (b and c). Each of the MZIs contains a Kerr medium in one of the arms that couples the internal b-mode to an external mode (a), which is initially in a coherent state $|\alpha\rangle$. The experimental set-up is illustrated in figure 2, where the upper part shows details of the first MZI and the lower one presents pictorially the sequence of MZIs.

Initially a single photon (mode b) and vacuum state (mode c) enter the first ideal 50/50 symmetric beam splitter (BS) of the MZI. The action of BS1 is described, in terms of the

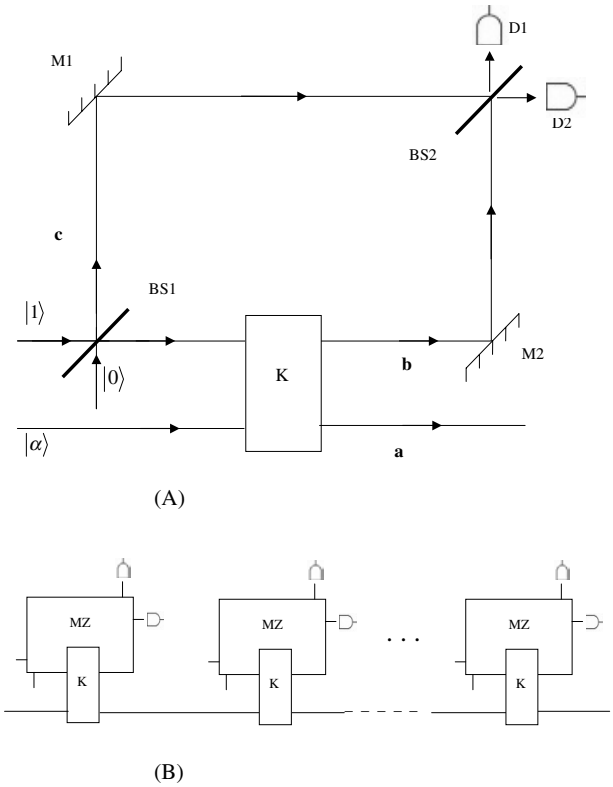

Figure 2. Schematic illustration of the experimental set-up for production of SCCSs as running modes; (A) shows details of the first Mach–Zehnder interferometer including a nonlinear Kerr medium, while (B) depicts the sequence of MZIs.

annihilation operators $\hat{b}$ and $\hat{c}$ for modes b and c, by the unitary operator [30]

$$\hat{R}_{bc} = \exp\left[i\frac{\pi}{4}(\hat{b}^\dagger\hat{c} + \hat{b}\hat{c}^\dagger)\right]. \qquad (5)$$

Just after the BS1, the (un-normalized) state of the system is given by $(|1\rangle_b|0\rangle_c + i|0\rangle_b|1\rangle_c)|\alpha\rangle_a$, where $|\alpha\rangle_a$ is the initial coherent state in mode a. The dispersive Kerr interaction between a- and b-modes is described by the interaction Hamiltonian [17]

$$\hat{H}_K = \hbar K\hat{a}^\dagger\hat{a}\hat{b}^\dagger\hat{b}, \qquad (6)$$

where K is proportional to the third order nonlinear susceptibility of the medium. Therefore the action of the Kerr medium is represented by the unitary operator

$$\hat{U}_K = \exp(-i\theta\hat{a}^\dagger\hat{a}\hat{b}^\dagger\hat{b}), \qquad (7)$$

where $\theta = Kl/v$, l being the length of the Kerr medium and v the velocity of light in the medium. So, after the medium and

just before the second beam splitter BS2, the (un-normalized) state of the system reads $|1\rangle_b|0\rangle_c|\alpha e^{-i\theta}\rangle_a + i|0\rangle_b|1\rangle_c|\alpha\rangle_a$. The second beam splitter implements the transformation

$$|1\rangle_b|0\rangle_c \to (|1\rangle_b|0\rangle_c + i|0\rangle_b|1\rangle_c)/\sqrt{2}, \tag{8}$$

$$|0\rangle_b|1\rangle_c \to (|0\rangle_b|1\rangle_c + i|0\rangle_b|1\rangle_c)/\sqrt{2}. \tag{9}$$

Thus, after BS2 the entangled state of the system is

$$|\Psi\rangle_{AF} = \tfrac{1}{2}\left[|1\rangle_b|0\rangle_c(|e^{-i\theta}\alpha\rangle_a - |\alpha\rangle_a) + i|0\rangle_b|1\rangle_c(|e^{-i\theta}\alpha\rangle_a + |\alpha\rangle_a)\right]. \tag{10}$$

If detector D1 (D2) fires, signalling the detection of the state $|1\rangle_b|0\rangle_c(|0\rangle_b|1\rangle_c)$, the a-mode is projected onto the state $|e^{-i\theta}\alpha\rangle_a - |\alpha\rangle_a$ ($|e^{-i\theta}\alpha\rangle_a + |\alpha\rangle_a$); so, taking the internal photon detected in D2 (mode c), the state projected in mode a is $|\Psi_1(\alpha, -\theta)\rangle$, as formerly suggested in [31].

Now, assume that a second MZ apparatus is aligned with the first one, again with a single photon in mode b and the vacuum in mode c, but with mode a in the state $|e^{-i\theta}\alpha\rangle_a + |\alpha\rangle_a$ which emerges from the first MZI. If the second Kerr medium is adjusted such that $\theta = \theta_2$, then the field–field entangled state in the second apparatus evolves as in table 1 with $|e\rangle_2$ ($|g\rangle_2$) replaced by $|1\rangle_b|0\rangle_c$ ($i|0\rangle_b|1\rangle_c$) and θ_1 (θ_2) changed to $-\theta_1$ ($-\theta_2$). Going further, considering a sequence of N MZIs, taking $\theta_j = \theta/2^{N-1}$ and assuming that all photons are detected by D2 (corresponding to the detection of the state $|0\rangle_b|1\rangle_c$), the outcome in mode a will be the state $|\Psi_N(\alpha, -\theta)\rangle$. Notice that $|\Psi_N(\alpha, \theta + 2\pi)\rangle = |\Psi_N(\alpha, \theta)\rangle$ so that these states coincide with the symmetrical superposition for the cases $\theta = \pm\pi$.

It is worth mentioning that the schemes for generating an SCCS in a cavity and as a running mode can be mapped into one another as alluded before. The beam-splitters in the second scheme play the role of the Ramsey zones in the cavity procedure while the atom–field interaction in C is simulated by the field–field effective dispersive interaction engendered by the Kerr medium. Furthermore, the ionization detection of the atomic state $|g\rangle$ is equivalent to the photon register in detector D2 and, naturally, the number of atoms crossing the cavity system corresponds to the number of aligned MZ apparatuses in the second case.

So far we have not analysed the real conditions to implement experimentally these schemes. Such a discussion will be postponed; firstly, we investigate the possibility that the SCCS states become specific highly excited Fock states, with fidelity close to unity, by looking at the dependence of their photon-number distributions on the parameters α and θ.

3. Generation of Fock states

We shall now investigate the possibility of generating highly excited number states as specific SCCSs. The photon-number distribution (PND), $P_{|\Psi\rangle}(n)$, of a given state of the field, $|\Psi\rangle$ say, corresponds to the fidelity between the state $|\Psi\rangle$ and the number state $|n\rangle$. Therefore, to investigate whether $|\Psi_N(\alpha, \theta)\rangle$ approaches a number state, analysing specific choices of the parameters α and θ, we look at how its PND depends on these parameters.

3.1. Photon statistics of SCCS

To obtain the PND of SCCS, we have to determine the normalization factor that appears in (4) by requiring that $\langle\Psi_N(\alpha, \theta)|\Psi_N(\alpha, \theta)\rangle = 1$. With α real, it is found that

$$\mathcal{N}_N(\alpha, \theta) = \left[2^N \exp(-\alpha^2)\mathcal{A}_N(\alpha^2, \theta)\right]^{-1/2}, \tag{11}$$

where

$$\mathcal{A}_1(\alpha^2, \theta) = e^{\alpha^2} + e^{\alpha^2\cos\theta}\cos(\alpha^2\sin\theta) \tag{12}$$

and, for $N \geqslant 2$,

$$\mathcal{A}_N(\alpha^2, \theta) = \mathcal{A}_1(\alpha^2, \theta) + \frac{1}{2^N}\sum_{l=1}^{J_N}(2^N - 2l) \times \{2e^{\alpha^2\cos(\theta l/2^{N-1})}\cos[\alpha^2\sin(\theta l/2^{N-1})] + e^{\alpha^2\cos(\theta+\theta l/2^{N-1})}\cos[\alpha^2\sin(\theta + \theta l/2^{N-1})] + e^{\alpha^2\cos(\theta-\theta l/2^{N-1})}\cos[\alpha^2\sin(\theta - \theta l/2^{N-1})]\}. \tag{13}$$

The PND for the SCCS is easily obtained by expanding the state given in equation (4) in the Fock basis. We have

$$P_N(n; \alpha, \theta) = |\langle n\,|\Psi_N(\alpha, \theta)\rangle|^2 = \mathcal{F}(|n\rangle, |\Psi_N\rangle) \tag{14}$$

where $\mathcal{F}(|n\rangle, |\Psi_N\rangle)$ stands for the fidelity between $|n\rangle$ and $|\Psi_N(\alpha, \theta)\rangle$, and

$$\langle n\,|\Psi_N(\alpha, \theta)\rangle = \frac{\mathcal{N}_N(\alpha, \theta)e^{-\alpha^2}\alpha^n}{\sqrt{n!}} \times \sum_{j=0}^{J_N}[e^{in\theta(1+j/2^{N-1})} + e^{in\theta(j/2^{N-1})}]; \tag{15}$$

performing the geometric summations above, one finds

$$P_N(n; \alpha, \theta) = \frac{(\alpha^2)^n\left[1 - \cos^2(n\theta)\right]}{2^{N-1}\mathcal{A}_N(\alpha, \theta)n!\left[1 - \cos(n\theta/2^{N-1})\right]}. \tag{16}$$

Notice that the probability normalization condition, $\sum_{n=0}^{\infty} P_N(n; \alpha, \theta) = 1$, leads directly to the series expansion (in powers of α^2) of the normalization functions (12), (13):

$$\mathcal{A}_N(\alpha^2, \theta) = \frac{1}{2^{N-1}}\sum_{n=0}^{\infty}\frac{(\alpha^2)^n}{n!}\frac{\left[1 - \cos^2(n\theta)\right]}{\left[1 - \cos(n\theta/2^{N-1})\right]}. \tag{17}$$

One sees that all the indicators of the photon statistics of $|\Psi_N(\alpha, \theta)\rangle$ are fully determined in terms of the function $\mathcal{A}_N(\alpha^2, \theta)$ and their derivatives ($\mathcal{A}_N^{(m)}$ denoting the order m one) with respect to α^2. In fact, one has

$$\langle\hat{n}\rangle = \alpha^2\frac{\mathcal{A}_N^{(1)}(\alpha^2, \theta)}{\mathcal{A}_N(\alpha^2, \theta)}, \tag{18}$$

$$\langle\hat{n}^2\rangle = \langle\hat{n}\rangle + \alpha^4\frac{\mathcal{A}_N^{(2)}(\alpha^2, \theta)}{\mathcal{A}_N(\alpha^2, \theta)}, \tag{19}$$

and so the Mandel factor [32] ($q = \langle\hat{n}^2\rangle/\langle\hat{n}\rangle - \langle\hat{n}\rangle - 1$) is given by

$$q_N(\alpha^2, \theta) = \alpha^2\left[\frac{\mathcal{A}_N^{(2)}(\alpha^2, \theta)}{\mathcal{A}_N^{(1)}(\alpha^2, \theta)} - \frac{\mathcal{A}_N^{(1)}(\alpha^2, \theta)}{\mathcal{A}_N(\alpha^2, \theta)}\right]. \tag{20}$$

The nature of the photon statistics of an SCCS oscillates between super- and sub-Poissonian behaviours as α^2 and θ are varied; this is illustrated in figure 3 for the state with $N = 4$.

To search for Fock states, one can look at the minimum of q, trying to get q_{min} as close as possible to -1. Here, we shall directly analyse the PND given by (16).

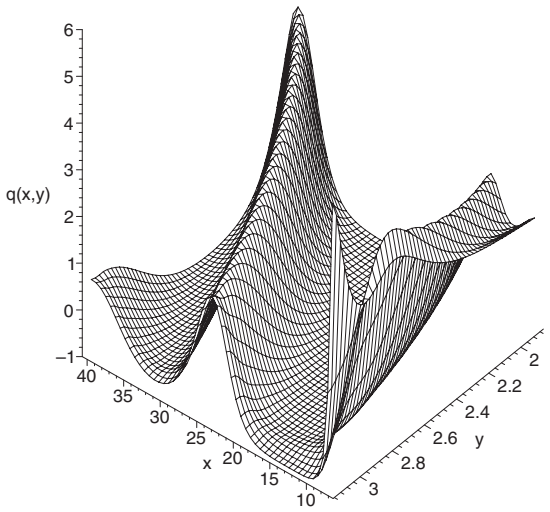

Figure 3. Mandel factor q as a function of α^2 $(=x)$ and θ $(=y)$ for the state $|\Psi_4(\alpha, \theta)\rangle$

3.2. Generation of number states

Now, we look at the expression of the PND in detail, searching for values of N, α and θ for which the fidelity between $|\Psi_N(\alpha, \theta)\rangle$ and some number state $|M\rangle$ is maximal, with the maximum value of $\mathcal{F}$ approaching 1.

A number state $|M\rangle$ is fully characterized by $P(n) = \delta_{n,M}$, so that we have to search for an SCCS which is almost zero for all n, except for $n = M$. From (16), we see that this never happens in an identical mathematical way. However, whenever θ is a rational fraction of π, $P_N(n; \alpha, \theta)$ presents (systematically) exact zeros regardless of the value of α. This feature is maximized by considering the symmetrical state where $\theta = \pi$; in this case, the only occupied number states are those for which n is a multiple of 2^N, that is, equation (16) reduces to

$$P_N(n; \alpha) = \frac{2^N(\alpha^2)^n}{\mathcal{A}_N(\alpha^2, \pi)n!}\delta_{n,2^N k}, \qquad (21)$$

with $k = 0, 1, 2, \ldots$.

The behaviour of the PND of the state $|\Psi_N(\alpha, \pi)\rangle$, as α is varied, is illustrated in figure 4 for the case of $N = 4$. One sees that, for small α, $|\Psi_N(\alpha, \pi)\rangle$ is essentially the vacuum state; as α increases, the occupation of the Fock state $|2^N\rangle$ grows at expense of that of $|0\rangle$; as α grows further, the participation of the vacuum state in $|\Psi_N(\alpha, \pi)\rangle$ begins to disappear while some occupation starts growing in the number state $|2^{N+1}\rangle$. Further increasing α, one sees that occupation of Fock states with n being a higher multiple of 2^N will occur. We also see from figure 4 that an optimal value of α ($\alpha_{\max}$) should exist for which the fidelity between $|\Psi_N(\alpha, \pi)\rangle$ and $|2^N\rangle$ is maximal. The values of α that maximize this fidelity are presented in table 3, for various values of N.

In this table, the optimal values of α are presented with two decimal places but, actually, the fidelity is not so sensitive to the precision on the value of α; in fact there is a plateau of values of α for which $|\Psi_N(\alpha, \pi)\rangle$ is rather close to $|2^N\rangle$. This can be seen from the plot of the Mandel factor, as in figure 3 for the case $N = 4$; there is a plateau, around $\alpha^2 = 12.8$, where the values of q_4 are very close to -1. Also, figure 4(c) shows

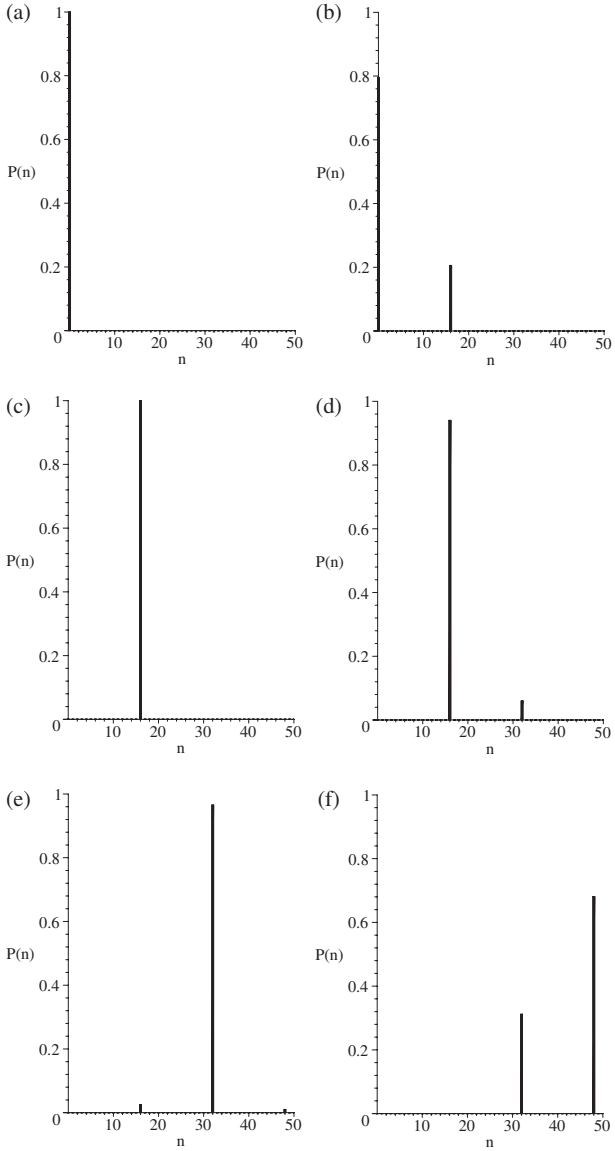

Figure 4. Photon-number distribution of states $|\Psi_4(\alpha, \pi)\rangle$, for some values of α: (a) $\alpha = 1.5$, (b) $\alpha = 2.5$, (c) $\alpha = 3.5$, (d) $\alpha = 4.5$, (e) $\alpha = 5.5$, (f) $\alpha = 6.5$.

Table 3. Optimal values of α and the associated fidelities between $|\Psi_N(\alpha_{\max}, \pi)\rangle$ and $|2^N\rangle$. The integer inside parentheses represents the number of decimal places for which the approximation is valid.

N	$\alpha_{\max}$	$\mathcal{F}(\lvert\Psi_N(\alpha_{\max}, \pi)\rangle, \lvert 2^N\rangle)$
2	2.01	0.799
3	2.61	0.982
4	3.58	1 (3)
5	4.96	1 (8)
6	7.33	1 (13)

that, for $\alpha = 3.5$ (which is slightly smaller than the optimal value $\alpha_{\max} = 3.58$), one already obtains a state which, to a high precision, coincides with the number state $|16\rangle$.

The sculpturing process of Fock states of the type $|2^N\rangle$ can be illustrated by presenting the PND of the states generated in each step when passing N atoms through the cavity or, for travelling modes, as the external field crosses the sequence of

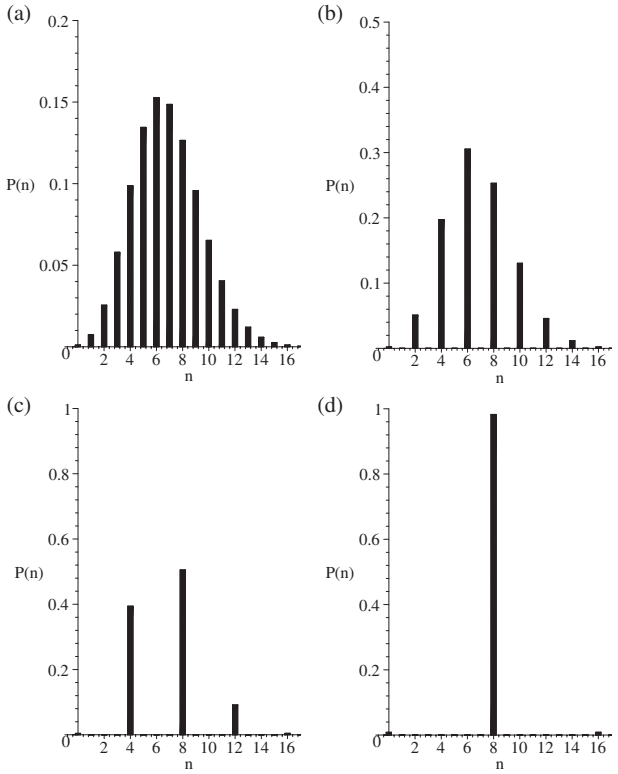

Figure 5. Evolution of the sculpturing process of the Fock state $|8\rangle$; in all these plots, we fixed $\alpha = 2.61$, and sub-figures (a)–(d) correspond to $N = 0$ (initial coherent state) up to $N = 3$.

MZIs. We show the sculpturing of the state $|8\rangle$ (corresponding to $N = 3$) in figure 5. In this case, the fidelity between the generated state and the number state $|8\rangle$ is high (about 98%), but one can still see that some occupation of the states $|0\rangle$ and $|16\rangle$ remains. For the case of the state $|16\rangle$ ($N = 4$), figure 4(c) already shows that we obtain this number state with fidelity equal to unity up to three decimal places.

For higher values of N, the fidelity between the states $|\Psi_N(\alpha_{\max}, \pi)\rangle$ and $|2^N\rangle$ becomes extremely close to unity, as shown in table 3. We present, in figure 6, the sculpturing process of the number state $|32\rangle$ by plotting the PND of the projected states as N goes from zero to five, with the (fixed) optimal value of α, $\alpha_{\max} = 4.96$; in this case the fidelity between the generated state and the state $|32\rangle$ is equal to unity within eight decimal places.

An important aspect, related to the generation of highly excited Fock states of the type $|2^N\rangle$, concerns the experimental feasibility of producing the states $|\Psi_N(\alpha_{\max}, \pi)\rangle$, both in a microwave cavity and as running waves.

Firstly, this demands good control of the values of the parameters α and θ. The precision on the value of α, as mentioned before, is not so important; varying α within a decimal place around the optimal value certainly would not affect our results. But this presupposes that the value of θ has been fixed as π. Distinct values of θ fundamentally change the state $|\Psi_N(\alpha_{\max}, \theta)\rangle$ as far the generation of Fock states is concerned; this is already indicated in figure 3, where one sees that diminishing the value of θ below π (say by 0.1) significantly raises the Mandel factor above -1.

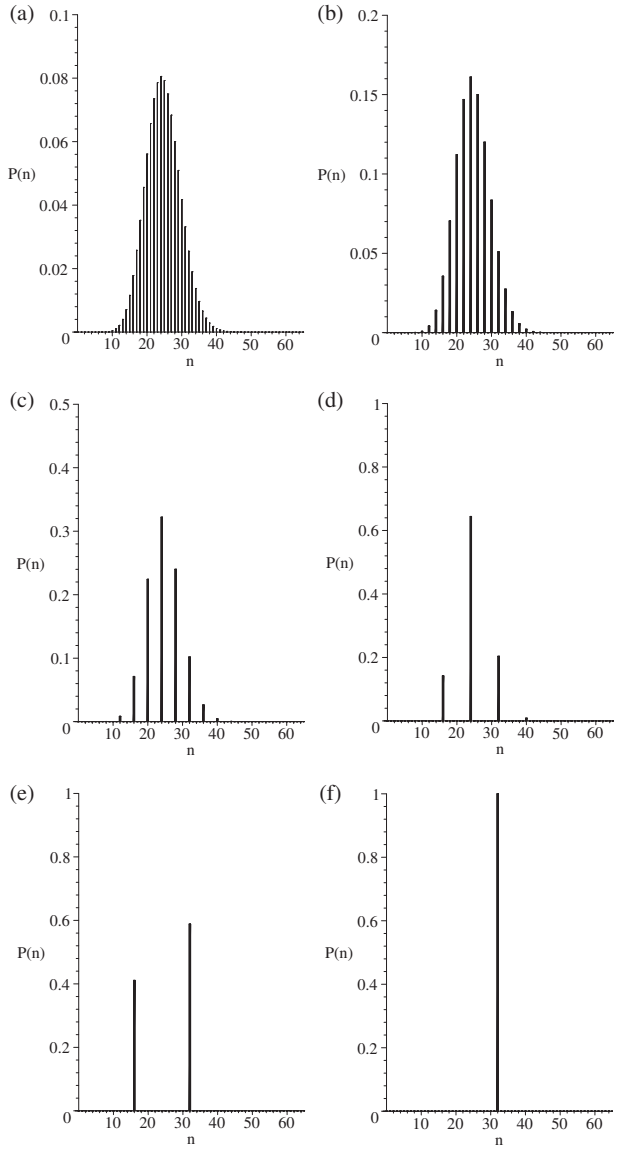

Figure 6. Evolution of the sculpturing process of the Fock state $|32\rangle$; in all these plots, we fixed $\alpha = 4.96$, and parts (a)–(f) correspond to $N = 0$ (initial coherent state) up to $N = 5$.

Fortunately, laboratory precision reaches the parameter θ in its first decimal place.

A π phase-shift in the field, induced by the passage of the first atom through the apparatus presented in figure 1, has been achieved in generating Schrödinger cat states in a cavity [33]. Besides this, one has to ensure that the second atom leads to a $\pi/2$ phase-shift in the field, the third one producing a shift of $\pi/4$ and so on. This requires adequate velocity selectors to choose appropriate speeds for atoms crossing the high-Q cavity. Also, delicate time switches should be coupled with fine microwave generators that properly adjust the intensities at which the Ramsey zones must operate in order to produce a $\pi/2$ pulse in the atomic states, before each atom enters the cavity. In this way, one can prepare the sequence of atoms engendering the desired phase-shifts in all steps of the process. But one has also to warrant that all Rydberg atoms are detected in their ground states. Roughly speaking, the probability that

N atoms are all detected in $|g\rangle$ is 2^{-N} and one has also to ensure that the time separation between the passage of two consecutive atoms is shorter than the decoherence time of the field already generated in the cavity. Therefore, subtle experimental aspects are involved in the production of highly excited Fock states in a cavity, but in principle the procedure can be implemented, at least for moderate values of N.

As far the generation of such states as running waves is concerned, some distinct aspects should be considered. The first point to be considered is the possibility of generating a phase-shift of π with the first MZ. For optical modes, to obtain such a phase-shift would require a very large Kerr nonlinear susceptibility or an extremely long medium [34]; but large nonlinearities are not yet available and long paths in the medium lead to strong dissipation effects. Although some suggestions to enhance the Kerr nonlinearity have been presented [35], this point is one of the greatest difficulties for the generation of Fock states of the type $|2^N\rangle$. Besides this aspect, one has to produce single-photon states to feed modes b of the MZ interferometers, align them and adjust the Kerr media to guarantee that the phase-shift produced by the jth MZI is given by $\pi/2^{j-1}$. Even under such restrictive conditions, some states of the type $|2^N\rangle$ might be created as travelling waves.

It should be pointed out that the success probability of generating the Fock state $|2^N\rangle$, in both experimental schemes, is only equal to 2^{-N} if one considers ideal atom and photon detectors. In this case, other sequences of detections (different from all atoms in $|g\rangle$ or all photons detected by D2) lead to other superpositions of circular coherent states, which are distinct pure states that do not approximate the desired Fock state; if this happens, the experiment must be repeated until the desired output is reached. However, in practice detectors are not ideal; while photodetectors with efficiency near 100% can now be constructed [36], the best efficiencies of atomic detectors are still around 70% [37]. Non-ideal detectors, as well as decoherence effects along the process, tend to create an uncontrolled mixed state output instead of the expected pure state; this aspect, which affects the production of whatever state (pure or mixed), is inherent to all generation schemes based on selective detection of states of part of the system, and challenges new technological advances.

It is worth mentioning that the method suggested in [25] requires M atoms crossing the cavity to generate an arbitrary equidistant superposition of $M+1$ coherent state and so would require 2^N-1 atoms to create the state $|\Psi_N\rangle$. Here, by dropping the generality, we are able to generate a specific superposition of 2^N coherent state components using solely N atoms which, by appropriate choice of parameters, corresponds to the highly excited Fock state $|2^N\rangle$.

3.3. Wigner representation

In order to check how coincident the states $|\Psi_N(\alpha_{\max},\pi)\rangle$ and $|2^N\rangle$ are, we now compare their Wigner phase-space representations. The Wigner function may be defined as the Fourier transform, $W(\beta)=\pi^{-1}\int \mathrm{d}^2\eta\exp(\eta^*\beta-\eta\beta^*)\chi(\eta)$, of the symmetrically ordered characteristic function of the density matrix of the state $\chi(\eta)=\mathrm{Tr}\{\rho\exp(\eta\hat{a}^\dagger-\eta^*\hat{a})\}$, where $\beta=x+\mathrm{i}y$ stands for a point in phase space.

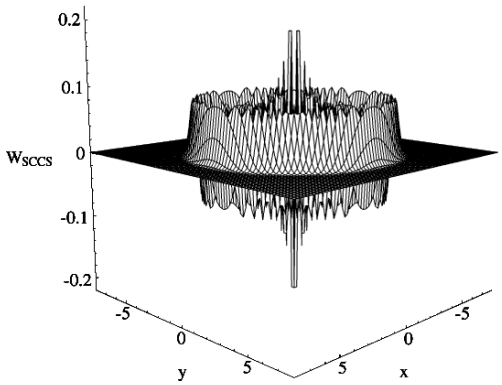

Figure 7. Wigner function for the SCCS with $N=5$ and $\alpha=4.96$, that is $|\Psi_5(4.96,\pi)\rangle$.

Considering the state (4) with $\theta=\pi$, after algebraic manipulations and Gaussian integrations, one obtains the Wigner function of the state $|\Psi_N(\alpha,\pi)\rangle$ in the form

$$W_{|\Psi_N\rangle}(\beta;\alpha)=\frac{\mathrm{e}^{-2\beta\beta^*}}{2^{N-2}\pi\mathcal{A}_N(\alpha^2,\pi)}\times\sum_{j,k=0}^{J_N}\left\{\mathrm{e}^{-\alpha_j\alpha_k^*}\cosh\left[2(\alpha_j\beta^*+\alpha_k^*\beta)\right]+\mathrm{e}^{\alpha_j\alpha_k^*}\cosh\left[2(\alpha_j\beta^*-\alpha_k^*\beta)\right]\right\}. \tag{22}$$

Such a function should be close to the Wigner function of the state $|2^N\rangle$ if one chooses for α the value $\alpha_{\max}$ which maximizes the fidelity between these states. In figure 7 we plot the Wigner function for the case $N=5$ taking $\alpha=\alpha_{\max}=4.96$.

On the other hand, the Wigner function of the Fock state $|n\rangle$ is given by

$$W_{|n\rangle}(\beta)=\frac{2}{\pi}(-1)^n\mathrm{e}^{-2\beta\beta^*}L_n(4\beta\beta^*), \tag{23}$$

where $L_n(z)$ stands for the Laguerre polynomial of order n. By simply looking at the plot of this function for $n=32$, it would not be possible to distinguish it from that in figure 7. To see any distinction one has to draw the difference between the Wigner functions of $|\Psi_5(4.96,\pi)\rangle$ and $|32\rangle$, which is done in figure 8. One sees that the largest difference between the values of these functions is of the order of 10^{-5} which cannot be detected in ordinary experiments reconstructing Wigner functions of states. Taking the case $N=4$, the coincidence between $|\Psi_4\rangle$ and $|16\rangle$ is a little smaller with $\max\{|W_{|\Psi_4\rangle}(\beta;3.58)-W_{|16\rangle}(\beta)|\}\simeq 3\times10^{-3}$, the maximum value of the Wigner functions being around 0.2. But considering larger values of N one obtains extremely high coincidence. For $N=6$, one has $\max\{|W_{|\Psi_6\rangle}(\beta;7.33)-W_{|64\rangle}(\beta)|\}\simeq 3\times10^{-9}$, with the maximum value of the Wigner functions being of the order of 0.1; thus, for any practical purpose, the state $|\Psi_6(7.33,\pi)\rangle$ is the same as the Fock state $|64\rangle$. From the preceding analysis, one sees that the coincidence between the states $|\Psi_N(\alpha_{\max},\pi)\rangle$ and $|2^N\rangle$, as indicated by the fidelity between them, occurs point to point in phase space, greatly increasing as N grows.

Actually, the comparison of the Wigner functions, searching for the circumstance where the maximum value of their difference tends to zero, constitutes a precise way to quantify the degree of coincidence between states. However, investigating whether a member of a family of

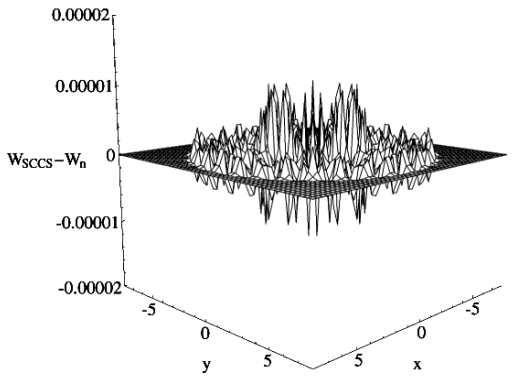

Figure 8. Difference between the Wigner functions of the SCCS $|\Psi_5(4.96, \pi)\rangle$ and the Fock state $|32\rangle$.

states is close to a given state using such a procedure is less operational than looking at the maximum of the fidelity between the considered states.

4. Conclusions

We have studied two complementary schemes for the generation of highly excited number states, one of them for stationary fields and the other for travelling waves. In the first case, a few (N) two-level Rydberg atoms are employed to prepare Fock states ($|2^N\rangle$) of trapped fields inside a high-Q microwave cavity. The method mimics a sculpturing process by which each atom discards the occupancy of a set of number components of a pre-existing superposition of circular states, gathering the photons inside the cavity in a smaller number of Fock states, until the Nth atom finally tailors the number state $|2^N\rangle$. This demands that we fix the parameter $\theta = \pi$ and optimize the intensity α^2 of the initial coherent state in the cavity to obtain the maximal fidelity between the generated state $|\Psi_N(\alpha_{\max}, \pi)\rangle$ and the number state $|2^N\rangle$. We have shown that for $N = 3$ the fidelity is greater than 98% and increases strongly as N grows; the comparison between the Wigner functions of these states firmly sustains this assertion.

We have also shown that the cavity scheme can be mapped into a running-wave procedure, allowing us to extend our results for travelling fields in the optical domain. To this purpose, a sequence of Mach–Zehnder interferometers, containing a Kerr medium in one arm, is used to couple an internal mode carrying a one-photon state to an initially coherent state in the external mode. As the external wave runs along the system, by properly adjusting the parameters involved, one ends up with a travelling state which coincides with the one generated in the cavity by passing a sequence of atoms.

Finally, we should mention that the process we have described permits us also to generate some specific superpositions of Fock states of the type $|k2^N\rangle$, where $k = 0, 1, 2, \ldots$. Methods for generating superpositions of a few number states ($c_0|0\rangle + c_1|1\rangle + \cdots + c_m|m\rangle$) as running waves, using arrays of beam-splitters, have already appeared in the literature [13]. The prescription presented here might also leads to the generation, both for trapped and travelling fields, of superpositions of the kind $A|k2^N\rangle + B|(k+1)2^N\rangle$. This can be seen (for example) from figure 4(b) where, for $N = 4$ and $\alpha = 2.5$ ($\theta = \pi$ fixed), one generates a state which approximates the superposition $\sqrt{0.8}|0\rangle + \sqrt{0.2}|16\rangle$ with a high fidelity. Optimizing the value of α around 2.5, one sees that such a fidelity can be made very high indeed. A thorough analysis of the possibility of generating such a kind of superposition state is in progress and will be presented elsewhere.

Acknowledgment

We thank CNPq (Brazil) for partially supporting this work.

References

[1] Bennett C H *et al* 1993 *Phys. Rev. Lett.* **70** 1895
Davidovich L *et al* 1994 *Phys. Rev.* A **50** R895
Bownmester D *et al* 1997 *Nature* **390** 575
Boshi D *et al* 1998 *Phys. Rev. Lett.* **80** 1121
Julsgaard B *et al* 2001 *Nature* **413** 400
[2] Turchette Q A *et al* 1995 *Phys. Rev. Lett.* **75** 4710
Kane B E 1998 *Nature* **393** 133
Chuang I L *et al* 1998 *Nature* **393** 143
Vandersypen L M K *et al* 2001 *Nature* **414** 883
[3] Cirac J I *et al* 1997 *Phys. Rev. Lett.* **78** 3221
Pellizzari T 1997 *Phys. Rev. Lett.* **79** 5242
Briegel H J *et al* 1998 *Phys. Rev. Lett.* **81** 5932
[4] Gisin N *et al* 2002 *Rev. Mod. Phys.* **74** 145
[5] Barnett S M and Pegg D T 1996 *Phys. Rev. Lett.* **76** 4148
[6] Bjork G and Sánchez-Soto L L 2001 *Phys. Rev. Lett.* **86** 4516
[7] Moussa M H Y and Baseia B 1998 *Phys. Lett.* A **238** 223
[8] Bergou J A, Hillery M and Yi D 1991 *Phys. Rev.* A **43** 515
[9] Avelar A T, Baseia B and de Almeida N G 2003 *J. Opt. B: Quantum Semiclass. Opt.* **6** 41
[10] Baseia B, Moussa M H Y and Bagnato V S 1997 *Phys. Lett.* A **231** 331
[11] Vogel K, Akulin V M and Schleich W P 1993 *Phys. Rev. Lett.* **71** 1816
Parkins A S *et al* 1993 *Phys. Rev. Lett.* **71** 3095
Law C K and Eberly J H 1996 *Phys. Rev. Lett.* **76** 1055
[12] Brune M *et al* 1990 *Phys. Rev. Lett.* **65** 976
Brune M *et al* 1992 *Phys. Rev.* A **45** 5193
[13] Dakna M *et al* 1998 *Phys. Rev.* A **59** 1658
Pegg D T, Phillips L S and Barnett S M 1998 *Phys. Rev. Lett.* **81** 1604
Villas Boas C J *et al* 2001 *Phys. Rev.* A **63** 055801
Valverde C *et al* 2003 *Phys. Lett.* A **315** 213
[14] Yurke B and Stoler D 1986 *Phys. Rev. Lett.* **57** 13
[15] Maeda M W, Kumar P and Shapiro J H 1986 *J. Opt. Soc. Am.* **3** 238
[16] Pereira S F *et al* 1987 *Phys. Rev.* A **38** 4931
[17] Imoto N, Haus H A and Yamamoto Y 1985 *Phys. Rev.* A **32** 2287
[18] Krause J *et al* 1989 *Phys. Rev.* A **39** 1915
Kozierowki M and Chumakov S M 1995 *Phys. Rev.* A **52** 4194
Domokos P *et al* 1998 *Eur. Phys. J.* D **1** 1
[19] D'Ariano G M *et al* 2000 *Phys. Rev.* A **61** 053817
Kilin S Y and Horosko D B 1995 *Phys. Rev. Lett.* **74** 5206
Leonski W, Dyrting S and Tanas R 1997 *J. Mod. Opt.* **44** 2105
Vidiella-Barranco A and Roversi J A 1998 *Phys. Rev.* A **58** 3349
Leonski W 1996 *Phys. Rev.* A **54** 3369
Paris M G A 1997 *Int. J. Mod. Phys.* B **11** 1913
[20] Nogues G *et al* 1999 *Nature* **400** 239
[21] Varcoe D T H *et al* 2003 *Nature* **403** 743
[22] França M, Solano E and de Matos Filho R L 2001 *Phys. Rev. Lett.* **87** 093601
[23] Zurek W H 1991 *Phys. Today* **44** 36
Julsgaard B *et al* 2001 *Nature* **413** 400

[24] Domokos P, Janszky J and Adam P 1994 *Phys. Rev.* A **50** 3340
Janszky J *et al* 1995 *Phys. Rev.* A **51** 4191
[25] Szabo S *et al* 1996 *Phys. Rev.* A **53** 2698
[26] Ragi R, Baseia B and Mizrahi S S 2000 *J. Opt. B: Quantum Semiclass. Opt.* **2** 299
[27] José W D and Mizrahi S S 2000 *J. Opt. B: Quantum Semiclass. Opt.* **2** 306
Souza Silva A L *et al* 2001 *Phys. Lett.* A **282** 235
[28] Gerry C C and Knight P L 1997 *Am. J. Phys.* **65** 964
[29] Malbouisson J M C and Baseia B 1999 *J. Mod. Opt.* **46** 2015
[30] Yeoman G and Barnett S M 1993 *J. Mod. Opt.* **40** 1497
[31] Gerry C C 1999 *Phys. Rev.* A **59** 4095
[32] Mandel L 1982 *Opt. Lett.* **4** 205
[33] Davidovich L *et al* 1996 *Phys. Rev.* A **53** 1295
[34] Sanders B C and Milburn G J 1992 *Phys. Rev.* A **45** 1919
[35] Agarwal G S 1989 *Opt. Commun.* **72** 253
Schmidt H and Imamoglu A 1996 *Opt. Lett.* **21** 1936
Franson J D 1997 *Phys. Rev. Lett.* **78** 3853
[36] Imamoglu A 2002 *Phys. Rev. Lett.* **89** 163602
James D F V and Kwiat P G 2002 *Phys. Rev. Lett.* **89** 183601
[37] Auffeves A *et al* 2003 *Phys. Rev. Lett.* **91** 230405